Journal of Materials Chemistry A

ROYAL SOCIETY OF CHEMISTRY

PAPER

View Article Online
View Journal | View Issue

Cite this: J. Mater. Chem. A, 2025, 13, 28368

A facile synthesis of bulk LiPON in solution for solid-state electrolytes†

Osma J. Gomez,[a] Adam Antar,[b] Alex T. Hall,[c] Leopoldo Tapia-Aracayo,[c] Joshua Seo,[a] Nam Kim,[a] Zihan Sun,[a] Ryan Lim,[a] Fu Chen,[a] Yue Li,[a] John Cumings,[c] Gary Rubloff,[cd] Sang Bok Lee,*[a] David Stewart*[c] and Yang Wang*[a]

Received 22nd April 2025
Accepted 10th July 2025

DOI: 10.1039/d5ta03196f

rsc.li/materials-a

We present a facile, solution-based approach to prepare bulk lithium phosphorus oxynitride (LiPON) utilizing a stepwise reduction between lithium *tert*-butoxide (LiO^{t}Bu) and a phosphazene base, diethyl phosphoramidate (DEPA), which are also precursors used in LiPON synthesis by atomic layer deposition (ALD). The study finds that the two ALD LiPON precursors can readily react upon mixing in THF at room temperature, which yields an ionically conductive solid powder that may be used as a solid-state electrolyte in solid-state batteries or as a material for surface coating. We conducted comprehensive characterization studies using solid-state nuclear magnetic resonance (SSNMR) spectroscopy, cryogenic transmission electron microscopy (cryo-TEM), matrix-assisted laser desorption ionization mass spectroscopy (MALDI-MS), X-ray diffraction spectroscopy (XRD), and X-ray photoelectron spectroscopy (XPS) to study the structure of this bulk LiPON material, which exhibits a composition closely resembling $LiPO_2N$. We propose a reaction mechanism of this bulk synthesized LiPON in a solution system.

Introduction

Lithium phosphorus oxynitride (LiPON) is a solid-state electrolyte material that has garnered significant attention in the field of lithium-ion batteries, particularly for thin-film and all-solid-state battery applications, since its discovery in the 1990s.[1] This polymeric material has an ionic conductivity in the range between 10^{-6} and 10^{-7} S cm^{-1}, which is affected by the stoichiometry (which can vary widely in N and Li molar ratios) and the crystallinity of the material.[2] Previous studies have shown that having more lithium and more nitrogen results in a greater number of crosslinking P–N bonds in the structure, which can facilitate the migration of Li^+ ions and lead to higher ionic conductivity.[3,4] Amorphous LiPON is also shown to have higher ionic conductivity than crystalline LiPON, due to higher Li^+ ion mobility.[5–7] LiPON offers a unique combination of properties that make it highly suitable for use in advanced energy storage devices, most importantly due to its wide electrochemical stability window, greater stability against Li metal due to the self-limiting formation of ionically conductive solid-electrolyte interphases, and lower sensitivity to air compared to sulfide solid-state electrolytes.[8–10]

While LiPON has been successfully synthesized using atomic layer deposition (ALD) and sputtering methods, which produce high quality thin films for solid-state electrolytes and artificial solid electrolyte interphases (ASEIs),[11–13] our group has been seeking an easy method for bulk LiPON synthesis that can be fast, low-cost techniques and more compatible with many electrochemical device fabrication processes. There have been very few reports on the fabrication of bulk LiPON or free-standing LiPON (FS-LiPON). López-Aranguren *et al.* fabricated crystalline LiPON *via* the ball milling method.[2] Cheng *et al.* synthesized free-standing thin film LiPON through multiple steps using spin coating and sputtering methods.[14] By enabling bulk LiPON synthesis, the fabrication of this solid-state electrolyte or coating layer can be greatly scaled up to different sizes and shapes to meet the demand of mass production in industry. In addition, solution-made LiPON may also work as a powder coating technique in the solution phase for solid-state electrolyte particles.

Here, our approach represents a new direction by simply mixing LiO^{t}Bu and DEPA, the two precursors used in ALD LiPON fabrication, in a solution environment.[11,15] The ALD process deploys the two precursor vapors intermittently to react to form atomic layers of the LiPON thin film. We hypothesize that this reaction should also occur in solution. In addition, an ALD process typically requires that a substrate or powder that is to be coated be placed in a vacuum chamber, and the LiPON thin film is grown at 300 °C, both of which limit the materials

[a]Department of Chemistry and Biochemistry, University of Maryland, College Park, MD 20742, USA. E-mail: ywang16@umd.edu
[b]Department of Mechanical Engineering, University of Maryland, College Park, MD 20742, USA. E-mail: steward@umd.edu
[c]Department of Materials Science and Engineering, University of Maryland, College Park, MD 20742, USA. E-mail: slee@umd.edu
[d]Institute for Systems Research, University of Maryland, College Park, MD 20742, USA

† Electronic supplementary information (ESI) available. See DOI: https://doi.org/10.1039/d5ta03196f

that can be coated.[16] Although it results in an extremely high-quality, conformal thin film, the ALD method makes it impractical for the layer to grow more than a few hundred nm thick.[17,18] These quantity and technical challenges make synthesizing LiPON by a scalable, solution-based method particularly desirable. To date, there have been no reported instances of LiPON synthesis using solution-based methods or employing the specific precursors we have chosen for this study.[19]

In this paper, we present the synthesis and characterization of a bulk LiPON powder using comprehensive spectroscopic and electron microscopy techniques. From this characterization, we propose reaction mechanisms for solution-based LiPON synthesis reactions, which show that they are a series of oxidation reactions of the phosphazene base facilitated by LiO^tBu. The electrochemical property of this solution-based LiPON was evaluated with electrochemical impedance spectroscopy (EIS). The precursors undergo polymerization reactions to form this bulk, free-standing, polymer LiPON with promising ionic conductivity that bodes well for its application in batteries.

Methodology

Materials

Diethyl phosphoramidate (DEPA, 98%), tetrahydrofuran (THF, anhydrous, ≥99.9%, inhibitor-free), *tert*-butanol anhydrous 99.5%, *n*-butyllithium solution (*n*-BuLi, 11 M in hexanes), hexane, mixture of isomers anhydrous 99.9%, and calcium hydride 97.0% powder were purchased from Sigma Aldrich. All reagents were used as received, without further purification.

Synthesis of lithium *tert*-butoxide (LiO^tBu)

LiO^tBu was synthesized using *tert*-butanol (11.94 mL, 124.8 mmol) added to 50 mL of hexane. Upon cooling to 0 °C, add *n*-butyllithium (11.35 mL, 11 M in hexane solution) in an argon atmosphere, and the resulting solution was stirred at room temperature for 2 hours to prepare a LiO^tBu solution. The solution was then dried to yield 14.982 g of LiO^tBu as a fine white powder. ^{1}H NMR (500 MHz, d-DMSO) 1.0053 (s, 9H).

Synthesis of solution-based LiPON

In-house synthesized lithium *tert*-butoxide (LiO^tBu) and diethyl phosphoramidate (DEPA) (Sigma Aldrich) were respectively dissolved in anhydrous tetrahydrofuran (THF) to make 1 M solutions. The two solutions were mixed together (1 : 1, v/v) at room temperature and stirred for 48 hours, uncovered, on a magnetic stir plate set at 1500 rpm to fully react and dry naturally at room temperature. The resulting LiPON dry paste was ground into a fine powder. All synthesis steps were carried out in an Ar-filled glovebox with <5 ppm O_2 and H_2O.

NMR instrumentation

The ^{1}H NMR spectrum was measured in deuterated DMSO on a Bruker AV 400 MHz using Me_4Si as the internal standard. Chemical shifts are reported in parts per million (ppm) downfield (δ) from Me_4Si. For ^{1}H NMR multiplicity (s = singlet, d = doublet, dd = doublet of doublets, t = triplet, q = quartet, br = broad, m = multiplet) is reported whenever possible. Solid-state ^{1}H, ^{7}Li, ^{13}C, ^{15}N, and ^{31}P NMR spectra were collected on a Bruker Advance NEO solid-state 500 MHz NMR spectrometer with a double resonance H/F-X probe. Briefly, samples were packed in a 3.2 mm outer diameter zirconia rotor with a Kel-F endcap. Solid-state ^{7}Li NMR spectra were collected using one pulse program with 2.5 μs $\pi/2$ pulse length, and the recycle delay was 2 s. Each ^{7}Li spectrum was collected with 512 or 1024 scans spun at 16 kHz and the line broadening for the spectrum was 0 Hz. All solid-state ^{13}C, ^{15}N, and ^{31}P NMR experiments were performed using cross polarization (CP) with magic angle spinning (MAS) techniques. The proton dipolar decoupling was achieved by applying continuous wave SPINAL-64 decoupling scheme on the ^{1}H channel during acquisition. The $\pi/2$ pulse length was 2.5 μs for ^{1}H, and the recycle delay was 5 s. The proton-carbon matched cross polarization ramp was at 50 kHz with 2, 3.5, 3.5 ms contact time for ^{13}C, ^{15}N and ^{31}P, respectively. Each ^{13}C spectrum was collected with 1024 scans spun at 10 kHz, and the line broadening for the spectrum was 25 Hz. Each ^{15}N spectrum was collected with 12 288 scans spun at 6 kHz, and the line broadening for the spectrum was 25 Hz. Each ^{31}P spectrum was collected with 512 scans spun at 10 kHz, and the line broadening for the spectrum was 20 Hz.

X-ray diffraction (XRD) instrumentation

X-ray diffraction (XRD) was conducted on a Bruker D8 Advance Bragg–Brentano diffractometer with a copper anode, a step size of 0.019716°, and a step time of 0.75 s. The wavelength used in the XRD was 1.54060 Å. Due to air sensitivity, the LiPON powder was sealed in a stainless steel sample dish covered with Kapton tape inside the Ar glovebox before being transferred to the diffractometer. A background XRD scan was performed on the sample dish with Kapton tape (but no powder) using the same measurement settings. During post-processing, the Kapton tape LiPON sample was scaled by 0.7 prior to subtraction from the solution-based LiPON powder sample.

Cryo-TEM sample preparation

Samples were prepared by dry application of LiPON powder onto Quantifoil holey carbon TEM grids inside an Ar glovebox. The samples were immediately submerged in liquid nitrogen upon removal from the glovebox.

Cryo-S/TEM imaging instrumentation

All cryo-TEM imaging was performed using a JEOL JEM-2100 transmission electron microscope operated at 200 keV. Cryo-TEM images were acquired on a Gatan ORIUS SC1000 charge-coupled device (CCD) camera. All imaging was performed at cryogenic temperatures using a Simple Origin Model 215 cryo transfer holder. Samples were loaded into the holder under liquid nitrogen before insertion into the TEM. Cryo-TEM images were collected at magnifications below 200 00× to minimize beam damage. Camera binning was set to 1 throughout. Exposure times varied from 0.3–0.5 s.

X-ray photoelectron spectroscopy (XPS)

All XPS data were collected using a Kratos Axis Supra+ XRD system using monochromatic Al Kα radiation with a photon energy of 1486.7 eV. The solution-made LiPON powder sample was sealed in the airtight sample holder in an Ar-filled glovebox and transferred to the XPS system for surface chemical analysis without air exposure. Survey spectra were collected using a 15 kV monochromatic Al Kα X-ray source in hybrid lens mode with a step size of 1 eV and a pass energy of 160 eV. High-resolution spectra were collected using a 15 kV monochromatic Al Kα X-ray source in hybrid lens mode with a step size of 0.1 eV and a pass energy of 40 eV. The powder sample was sputtered in the XPS chamber to remove any degraded surface layers. The sputtering gun used was a multi-mode Ar gas cluster ion source, and a 10 k eV Ar 1000+ cluster was used for sputtering.

Sputtering occurred in stages to assess when the surface layer had been passed. Sputtering time for each step was 1 min, 3 min, 3 min, respectively, and 7 min in total. The sputtering rate is approximately 3 nm min^{-1}. The XPS spectra presented in the manuscript were all collected after 7 min of sputtering, thus with about 20 nm of the surface layer removed. XPS data were analyzed using the CasaXPS software, with quantification performed using peak areas normalized by standard photoionization cross sections corrected for our instrument geometry and a Shirley background for all high-resolution peaks. All spectra were calibrated to the C–C/C–H peak at 284.8 eV.

Matrix-assisted laser desorption ionization mass spectrometry (MALDI-MS)

The MALDI measurements were performed on a Bruker Autoflex MALDI-TOF mass spectrometer. Solution-made LiPON and the precursors LiO^tBu and DEPA were respectively dissolved in THF solvent to make 0.1 M solutions. The mass spectra were obtained in linear positive mode with 2-[(2*E*)-3-(4-*tert*-butylphenyl)-2-methylprop-2-enylidene]malononitrile (DCTB) in THF as the matrix. The mass range scanned was from 500 to 10 000 Daltons.

Electrochemical testing

To measure the ionic conductivity of solution-made LiPON, ground LiPON powder was sandwiched between sheets of Au foil (as ion blocking current collectors) and pressed at 60 °C and 300 MPa into 1.0 mm thick pellets, 12.7 mm in diameter. The Au/LiPON/Au pellet was then closed in a split cell (15 mm ID) and placed in an isothermal oven. Electrochemical impedance spectroscopy (EIS) testing was conducted at open circuit potential using a Bio-Logic VSP potentiostat with a frequency range from 1 MHz to 100 mHz and a 10 mV amplitude. The measurements were carried out at 20.0 °C and then again at 60.0 °C. EIS data were processed and compared to simulated electrochemical circuits using EC-lab software. EIS models were fit to a circuit model containing two resistor/constant phase element parallel pairs in series with each other, representing the impedance of the Au/LiPON interface and bulk LiPON, respectively (see Fig. S5†).

Results and discussion

The general synthetic scheme for the synthesis of LiPON is shown in Fig. 1. The addition of LiO^tBu to DEPA in THF results in a homogeneous, opaque, viscous white gel within 30 seconds. This is attributed to a reduction reaction occurring between LiO^tBu and DEPA upon mixing in THF. The proposed mechanism is illustrated in Fig. 1. Once the prepared powder is obtained, the sample is then hand ground for material characterization.

Proposed mechanism

An effective nanostructured polymer network was developed. This linear polymer electrolyte can easily be synthesized from a Schwesinger base, diethyl phosphoramidate (DEPA) and lithium *tert*-butoxide (LiO^tBu), as shown in Fig. 1.

The polymerization mechanism occurs in several stages, as illustrated in Scheme 1. First, in the initiation phase, lithium *tert*-butoxide serves as a reducing agent that converts the DEPA monomer into its anionic form. During propagation, this activated anionic DEPA attacks another DEPA monomer through nucleophilic addition, extending the polymer chain and generating lithium ethoxide as a byproduct. The lithium ethoxide doesn't remain idle – it participates by reducing additional amine groups, facilitating further polymer growth. The process becomes cyclical, with both lithium ethoxide and the remaining lithium *tert*-butoxide continuously activating and incorporating unreacted DEPA monomers. This cycle persists until all lithium *tert*-butoxide is consumed, progressively building the linear LiPON polymer through alternating reduction and substitution steps.

Solid-state nuclear magnetic resonance (NMR) spectroscopy differs significantly from solution NMR in sample preparation and spectral characteristics. Unlike solution NMR, which uses deuterated solvents and produces sharp peaks from completely

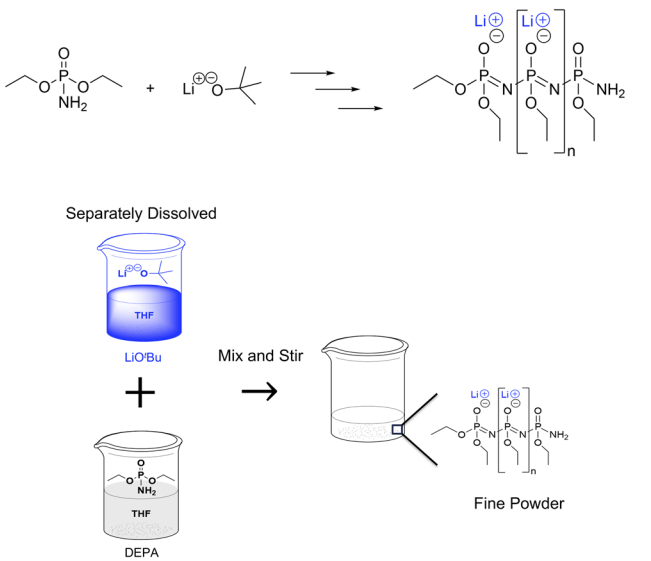

Fig. 1 Synthesis of bulk LiPON.

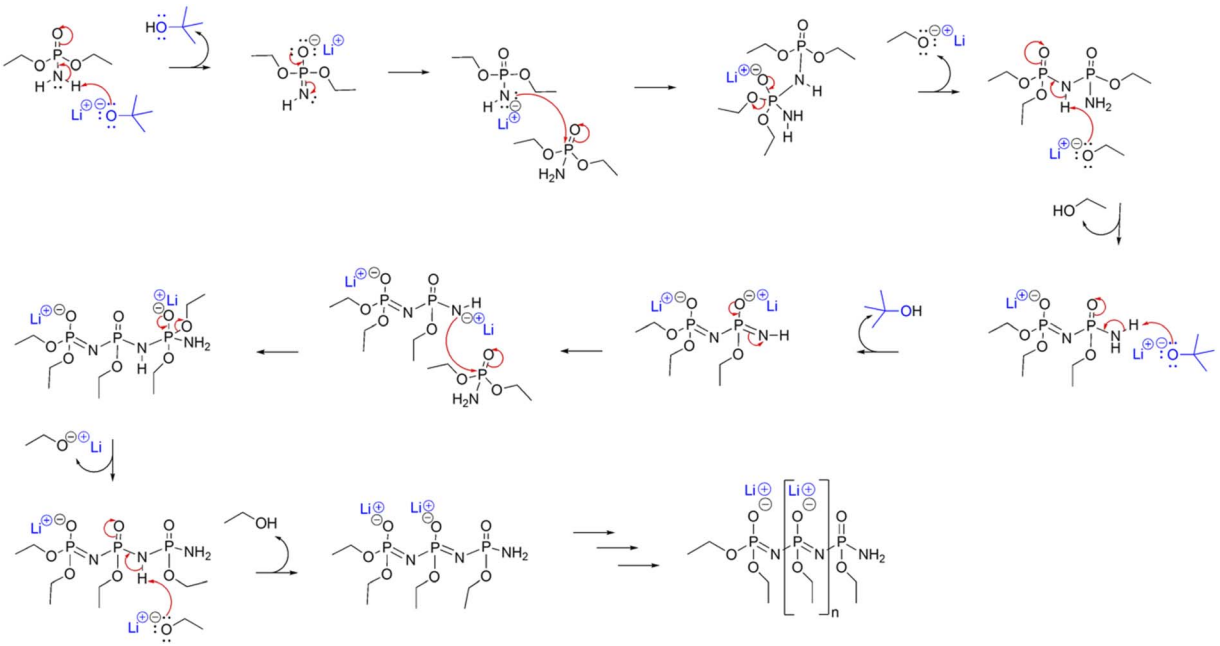

Scheme 1 Proposed mechanism of the reaction occurring between LiO^{t}Bu and DEPA in THF to form the as-prepared LiPON sample.

dissolved samples, solid-state NMR analyzes solid and semi-solid materials. This results in broader peaks due to anisotropic interactions that reflect the orientation-dependent properties of the sample.[20] To overcome these challenges, solid-state NMR employs cross polarization (CP) with magic-angle spinning (MAS) techniques, which help obtain high-resolution spectra and extract detailed structural information about solid and semi-solid materials at the atomic level.[21]

Validation of the product by solid-state NMR

The ^{13}C SSNMR spectra (Fig. 2a) show the complete consumption of LiO^{t}Bu (blue spectrum). The presence of DEPA (green spectrum) precursor's ethoxy carbon groups is confirmed by a prominent methyl (C_1) signal at 18 ppm and a symmetric doublet (C_2) signal at 60 ppm. It is evident that the ethoxy groups in the solution-based LiPON originated from the DEPA precursor (red spectrum) with peak asymmetry attributed to interactions with neighboring nuclei.[22]

In Fig. S1,† the ^{1}H SSNMR spectra of LiPON and its two precursors, LiO^{t}Bu and DEPA, are presented. While the ^{1}H SSNMR spectrum of solution-based LiPON exhibits less defined peaks (showing broad splitting patterns) compared to solution NMR, which is characteristic of solid-state samples,[23] it shows qualitatively the ~2 : 3 ratio of protons from the –O–CH_2–CH_3 group. The ^{7}Li SSNMR spectra (Fig. 2b) reveal contrasting lithium environments between the precursor and final product: (1) LiO^{t}Bu precursor (blue spectrum) shows a single (Li_1) signal indicating one uniform lithium environment. (2) Solution-based LiPON (red spectrum) shows a broad, weak asymmetric split (Li_1 and Li_2), suggesting two distinct lithium environments, which is likely due to different resonance arrangements in the polymerized structure mechanism. ^{7}Li also has a significant quadrupolar moment, which leads to broader signals and more complex splitting patterns, especially in asymmetric environments.[24] While CP-MAS improves resolution, it cannot fully eliminate asymmetric splitting for ^{7}Li. Additional analytical techniques, such as XPS, were considered for accurate analysis of complex lithium-containing systems.

The ^{15}N SSNMR spectra (Fig. 2c) show different nitrogen environments between the precursor and product: (1) DEPA precursor (green spectrum) exhibits a single broad peak (N_1) around 33 ppm, indicating one unique nitrogen environment. (2) Solution-based LiPON (red spectrum) shows symmetric peak splitting (N_1) around 25–40 ppm, which differs from the ^{7}Li solution-based LiPON NMR result. This symmetric splitting pattern can be attributed to strong quadrupolar interactions arising from the non-spherical charge distribution within the nitrogen nucleus. These interactions become particularly prominent when molecular motion in solution fails to completely average out the surrounding electric field gradient.[25] The resulting spectrum displays symmetric, distributed peaks around the resonance frequency, with their positions dependent on the molecule's orientation within the magnetic field.

The ^{31}P SSNMR spectra (Fig. 2d) reveal (1) the DEPA precursor (green spectrum) as a single clear phosphorus peak (P_1) at ~12 ppm. (2) Polymerized LiPON (red spectrum) shows asymmetric splitting (P_1 and P_2) between 17 and 30 ppm, which is very different from the ^{7}Li LiPON pattern.[2,26] This asymmetry can arise from several factors. First, during the Cross-Polarization (CP) process, magnetization may transfer unevenly to different ^{31}P environments. Second, when using moderate Magic Angle Spinning (MAS) speeds, anisotropic interactions may not be fully averaged out, leading to asymmetric peak shapes and spinning sidebands. Third, in complex materials such as LiPON, multiple phosphorus environments can

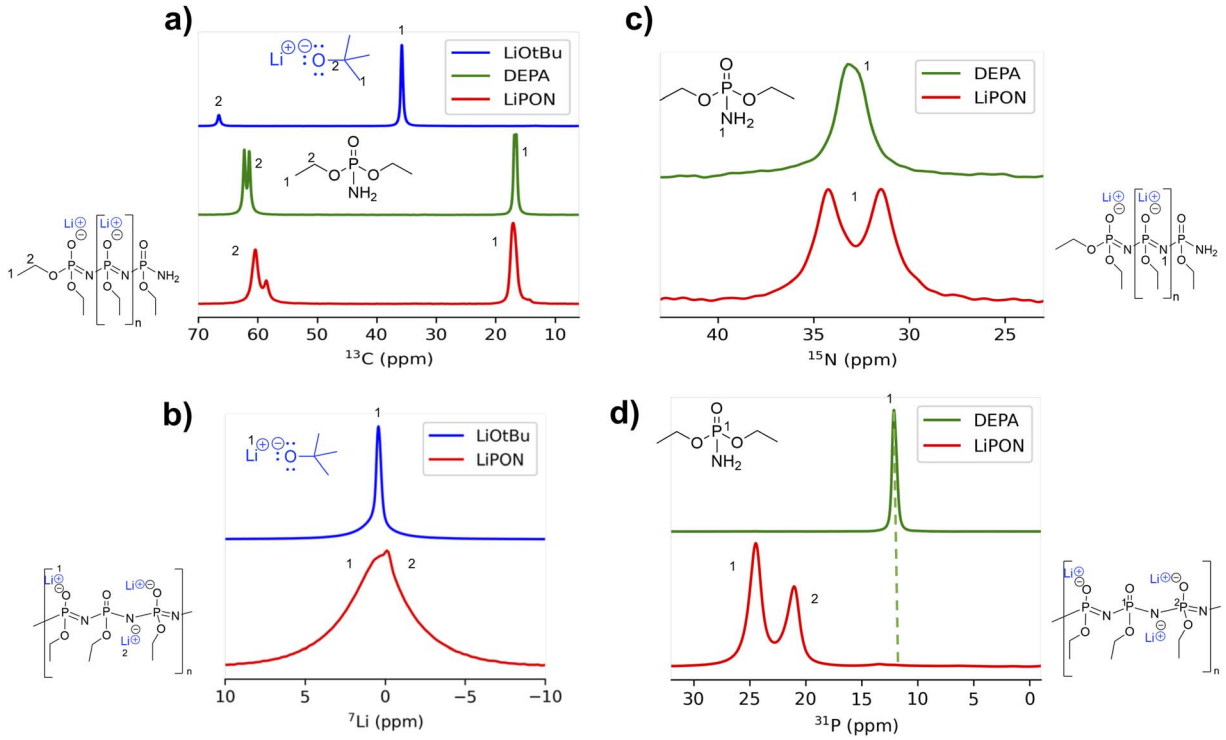

Fig. 2 All samples were analyzed individually using a 3.2 mm rotor with ~10 mg sample size. The analyses compared the LiPON polymer network product against its precursors (LiO^{t}Bu and/or DEPA). (a) CP-MAS 1D ^{13}C spectra stack comparison between both precursors and LiPON. (b) CP-MAS 1D ^{7}Li NMR spectra stack comparison between the LiO^{t}Bu precursor and LiPON at 6 kHz MAS rate, $d1 = 5$ s, $p1 = 2.5$ s, and NS = 64, run separately. (c) CP-MAS 1D ^{15}N NMR spectra stack comparison between the DEPA precursor and LiPON at 6 kHz, referenced to $^{15}NH_4Cl$ in saturated solution (25.3 ppm), run separately. (d) CP-MAS ^{31}P NMR spectra stack comparison between the DEPA precursor and LiPON.

produce overlapping signals with distinct chemical shifts and anisotropies, creating an overall asymmetric appearance. Although ^{31}P is not a quadrupolar nucleus, its coupling with nearby quadrupolar nuclei can affect the spectral features.[27] Additionally, ^{31}P can interact with neighboring nuclei (especially protons) through dipolar coupling. While CP-MAS techniques help reduce these dipolar interactions, incomplete averaging may contribute to the observed peak asymmetry.

The ^{13}C solution-based LiPON spectra correlate with our proposed mechanism since we expect there are repeating ethoxy groups throughout the polymer chain. The movement of the Li cation throughout the proposed mechanism is due to resonance, as shown in Scheme 1 and evident in the ^{7}Li NMR. Also, as suggested by the mechanism, the recurring presence of nitrogen throughout the polymer format can be seen in the resonance structure in our ^{15}N spectra. Finally, the shifting of Li^+ from O to N in the polymer can be seen to affect the resonance structure in the ^{31}P solution-based LiPON spectra, creating an asymmetry in the split peak.

Formation of rod-like amorphous particles (XRD and TEM)

X-ray diffraction (XRD) analysis was conducted to evaluate the structural characteristics of LiPON powder at room temperature without exposure to air and under inert conditions, as shown in Fig. 3a. The sample was assembled and sealed inside an Ar-filled glove box before being transferred for XRD measurement. The XRD revealed a substantial amorphous phase, based on the presence of the broad diffraction background between 5 and 30°. Comparison with the current International Crystallographic Structure Database (ICSD) and other prevalent compounds in the literature, such as Li_2O, Li_3PO_4, and Li_2CO_3, found that our synthesized LiPON did not match any existing known phases, as shown in Fig. S3(a–f†).[28] This systematic comparison substantiates the amorphous structure of our synthesized LiPON.

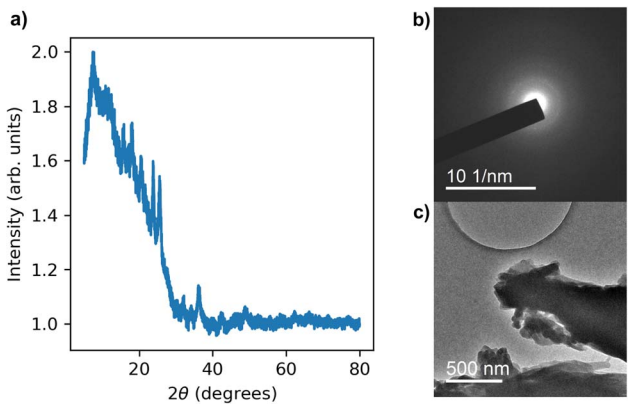

Fig. 3 (a) XRD pattern, (b) TEM diffraction pattern and (c) high resolution TEM image of solution-based LiPON.

Cryogenic transmission electron microscopy (cryo-TEM) diffraction patterns collected from the LiPON particles and aggregates were amorphous and are in good agreement with the XRD results. The position of the amorphous ring in the SAED image shown in Fig. 3b agrees with the broad amorphous hump in the XRD pattern shown in Fig. 3a. These results were consistent with previously reported XRD and electron diffraction patterns of thin-film LiPON in the literature.[29] A small amount of crystalline intensity, originating from unwanted side reactions with water and ice from the freezing process, was identified in the electron diffraction data. There is only one identifiable diffraction ring in the pattern shown, corresponding to a *d*-spacing of ~0.36 (±0.01) nm. We do observe a diffraction peak in the XRD at ~25.5°, which is approximately the Bragg angle that corresponds to this *d*-spacing. This could suggest that the unidentified crystalline phases(s) measured during XRD are isolated impurities and that the intended LiPON product is near amorphous. Further study is required with less air exposure and perhaps a higher purity product.

Fig. 3c shows that the synthesis formed rod-like particle aggregates, with some individual particles visible on the carbon support film surface. The particles varied in size, ranging from the smallest at approximately 150 nm in length and 50 nm in width, to the largest exceeding one micron in length with widths of several hundred nanometers.

Chemical bonding *via* XPS

We used XPS to study the chemical composition and chemical bonds of solution-made LiPON and Ar^+ sputtering for depth profiling, so we can remove the surface layer as much as possible and focus on the chemical composition of bulk LiPON.

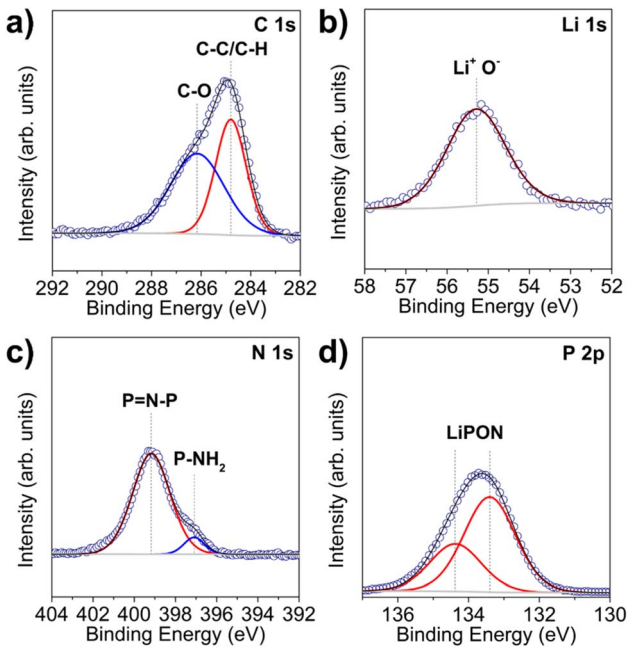

Fig. 4 High-resolution XPS (a) C 1s, (b) Li 1s, (c) 1s, and (d) P 2p spectra of solution-made LiPON after 7 minutes of Ar^+ sputtering.

The high-resolution C 1s, Li 1s, N 1s, and P 2p XPS spectra are shown in Fig. 4a–d after 7 minutes of Ar^+ sputtering.

The C 1s spectrum shows that there is common adventitious carbon and C–O (from the glove box atmosphere) that is still present between powder grains even after sputtering. The quantified atomic percent of C is 21.90%. As evidenced by our NMR results and the XPS P 2p spectrum here, some of the C–O components can also be ascribed to a small amount of residual DEPA in the sample. Fig. 4b shows the Li 1s spectrum, which only displays one single Li^+ peak.

As shown in the N 1s spectrum (Fig. 4c), the most prominent component has a binding energy (BE) of 399.14 eV, which corresponds to the P=N–P structure of LiPON shown in Scheme 1, while the much smaller peak at 397.15 eV corresponds to the residual DEPA, which has a primary amine group connected to P.[16] The quantification shows that this low BE peak is only 9.22 at% of the whole, so the amount of residual DEPA is small.

Fig. 4d shows the P 2p spectrum, where only one phosphorus species is identified, despite the N 1s spectrum confirming that there is a small amount of residual DEPA. This result could be due to the fact that the LiPON structure, or the repeating unit of LiPON that contains P, has an extremely similar structure to DEPA, where the only difference is the presence of a P=N bond in LiPON and a P=O bond in DEPA. In both LiPON and DEPA molecular structures, P is at the center of a tetrahedron, with the vertices being 3 O and 1 N in LiPON and 2 O and 2 N in DEPA, respectively. Despite the electronegativity difference between N and O, with the valence electron of P being delocalized in this tetrahedral structure, the difference in the electron-withdrawing effect on P between the two structures may be very small. Considering the trace amount of DEPA leftover and the roughly 2 eV large full width at half maximum (FWHM) of the P peaks, it might not be enough to differentiate LiPON and DEPA peaks in the P 2p spectrum; thus, they show up as a broad enveloped peak as we observe. Overall, the XPS peak shapes and positions agree well with previous XPS studies of LiPON, including the ones using the same precursors.[16]

In addition, we conducted quantification of the atomic percent of each element, and we found that overall, the bulk LiPON has a formula of $Li_{1.14}PO_{2.55}N_{0.58}C_{1.49}$. Some components that contain C and O can be attributed to adventitious carbon and general surface contamination from the glove box. It is notable that the formula derived from XPS quantification does not perfectly align with the theoretical structure of LiPON, which should be $LiPO_2NC_2H_5$ based on the proposed mechanism. This has also been the case in other synthesized bulk LiPON results.[2,14] It is likely because the reactions to form LiPON are far less fine-tuned compared to chemical deposition or sputtering methods, which are controlled at the nanoscale. Nonetheless, our results show an almost clean composition of LiPON, which has a well-defined structure that reflects our NMR characterization results. These results showed the C–C bond from the ethyl group originally from DEPA and the C–O bond that is the ethyl group that is connected to the O in the PO_2N_2 tetrahedral structure in the polymer chain, which points towards possible refinement directions.

We conducted MALDI-MS analysis to examine the phenomenon wherein the mixture turned into a viscous white gel when the two precursor solutions were mixed together, which we suspected was a polymerization reaction, and the solution-made LiPON was in the form of a polymer. Fig. S4a† shows the MALDI-MS spectrum with an m/z range from 0.5 kDa to 10 kDa. It needs to be noted first that LiPON has very low solubility in most solvents, including THF; thus, the actual concentration of LiPON in the testing sample is expected to be far less than the 0.1 M that we intended based on the amount of LiPON we added to the THF solvent. The very weak signal above background can be seen in Fig. S4a.† Nonetheless, it still clearly shows molecular peaks (*e.g.* individual polymer chains) in the high molecular weight (m/z) region, confirming that solution-made LiPON is indeed a polymer, and the synthesis was a polymerization reaction. We also used MALDI-MS to analyze the two precursors LiO^tBu and DEPA. As their results show in Fig. S4b and c,† neither showed any polymer peaks in the high m/z region resembling what we see in the solution LiPON spectrum. We did not conduct more detailed investigations of the gaps between the molecular peaks, mainly because MALDI sample preparation must be carried out under ambient conditions, which will inevitably expose the air-sensitive LiPON samples to moisture in the air as well as matrix chemical DCTB for more than 30 minutes at minimum. It has been studied that LiPON undergoes degradation when it reacts with water, which will render the repeating unit analysis inaccurate, if not impossible.[30,31] In any case, the polymeric natured molecular peaks in the high m/z region are observed in the LiPON MALDI spectrum but not in DEPA or LiO^tBu spectra.

Ionic conductivity by EIS

At last, we pressed ground LiPON powder into 1.0 mm thick pellets with Au foil as current collectors to measure the ionic conductivity of the solution-made LiPON in fully solid form using electrochemical impedance spectroscopy (EIS). We measured the EIS at 20.0 °C and 60.0 °C, and the results can be seen in Fig. S4† and 5, respectively. At 20.0 °C, the ionic conductivity of LiPON is lower with a lot of noise at the lower frequency region, in the transition from the rough semicircle figure (charge transfer impedance of bulk LiPON) to the straight line tail (diffusion in imperfectly blocking electrodes). As a result of the noise, we were not able to apply our equivalent circuit model (Fig. S6†) to fit the EIS spectrum.[32] But from the shape and size of the semicircle, we were able to estimate that the impedance of this 1.0 mm thick, 12.7 mm diameter LiPON pellet is roughly 700 kΩ, by which the ionic conductivity of solution-made LiPON is around 1×10^{-7} S cm^{-1}, which is not far from most sputtered or ALD deposited LiPON.[2,11]

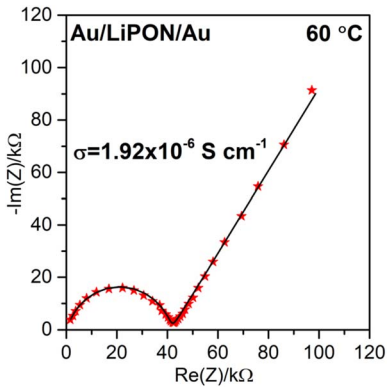

Fig. 5 EIS spectrum of the Au/LiPON/Au block electrode cell measured at 60.0 °C.

We then measured the ionic conductivity of solution-made LiPON at 60.0 °C, and the EIS spectrum can be seen in Fig. 5. At 60.0 °C, we did not observe the same noisy conditions at lower frequency, and the spectrum is clean. We were able to fit this spectrum with our equivalent circuit model (Fig. S5 and Table S1†) and based on the deconvoluted impedance result, we were able to calculate the ionic conductivity of the solution-made LiPON as 1.92×10^{-6} S cm^{-1} at 60.0 °C, as it is in line with most of the reported results in the literature. Considering the novel fabrication method we employed (without a systematic study to optimize the synthesis process), this ionic conductivity value is very encouraging and bodes well for many potential applications of this solution-made LiPON in the field of batteries.

Conclusion

We developed a novel solution-based synthesis method for solution-based LiPON utilizing LiO^tBu as an initiator to reduce DEPA monomers, generating anionic DEPA species. The polymerization proceeds through nucleophilic attack between the activated anionic DEPA and DEPA monomers, with LiOEt and LiO^tBu facilitating continuous reduction until complete consumption of LiO^tBu, resulting in the formation of sub-millimeter aggregates of LiPON polymer particles. Characterization using SSNMR and XPS confirmed the chemical structure and bonding environment, with peaks and binding energies consistent with those previously reported in the literature. Structural analysis using cryo-TEM and XRD revealed an amorphous polymer structure with particle dimensions ranging from 150 nm × 50 nm at their smallest to over 1 μm in length with widths of several hundred nanometers. The polymeric nature was confirmed through MALDI, while EIS measurements at 60 °C demonstrated an ionic conductivity of 1.92×10^{-6} S cm^{-1} for the pressed powder. This novel and facile solution-based synthesis route provides a brand new methodology for future free-standing, bulk synthesis of phosphazene compounds that may be used as both solid-state electrolytes and coating layers in beyond-Li energy storage devices, which until recently could only be fabricated on a limited scale using technically advanced yet challenging sputtering or atomic layer deposition method.

Data availability

Data for this article are available at Digital Repository at the University of Maryland (DRUM) at **https://doi.org/10.13016/uzs5-ziny**.

Author contributions

O. G., D. S., and Y. W. planned the research. S. L., D. S., and Y. W. developed the concepts. J. S., N. K., and R. L. collected the preliminary data. O. G. and Y. W. wrote the manuscript. O. G. and A. A. synthesized the precursors and the materials. O. G., A. T. H., L. T-A., Z. S., Y. L., D. S., and Y. W. conducted characterization studies and electrochemical testing. O. G., A. T. H., F. C., Y. L., J. C., G. R.; D. S., and Y. W. analyzed and interpreted the data and contributed to discussions during the process of writing the manuscript. All authors have given approval to the final version of the manuscript.

Conflicts of interest

The authors declare no competing financial interest.

Acknowledgements

The work was primarily supported by the U.S. Department of Energy, Office of Science, Office of Basic Energy Sciences under Award Number DE-SC0021070 for the synthesis of materials, characterization, electrochemical measurement and discussions, with additional support for synthesis idea and method discussion from the U.S.-Israel Energy Center Program, managed by the U.S.-Israel Binational Industrial Research and Development (BIRD) Foundation. We also acknowledge the support of the Maryland NanoCenter and the University of Maryland Department of Chemistry Instrument Core Facilities. We thank the Analytical NMR Service & Research Center at the University of Maryland, College Park for the use of solution and solid-state NMR spectrometers (supported by award NSF-1726058). O. G. acknowledges support provided by the Dolphus E. Milligan Graduate Fellowship through the National Institute of Standards and Technology (NIST). A. T. H. and J. C. acknowledge support from the Center for Enhanced Nanofluidic Transport (CENT), an Energy Frontier Research Center funded by the U.S. Department of Energy, Office of Science, Basic Energy Sciences, under Award # DE-SC0019112 for the TEM analysis and discussion. We extend our gratitude to Dr Andrei Vedernikov and Andrew Norris for providing training and access to their Schlenk line apparatus laboratory, enabling the synthesis of our in-house lithium *tert*-butoxide under inert conditions.

References

1 J. B. Bates, N. J. Dudney, G. R. Gruzalski, R. A. Zuhr, A. Choudhury, C. F. Luck and J. D. Robertson, *J. Power Sources*, 1993, **43**, 103–110.
2 P. López-Aranguren, M. Reynaud, P. Głuchowski, A. Bustinza, M. Galceran, J. M. López del Amo, M. Armand and M. Casas-Cabanas, *ACS Energy Lett.*, 2021, **6**, 445–450.
3 J. B. Bates, N. J. Dudney, G. R. Gruzalski, R. A. Zuhr, A. Choudhury, C. F. Luck and J. D. Robertson, *Solid State Ionics*, 1992, **53–56**, 647–654.
4 L. A. Green, *Scilight*, 2022, **2022**, 071104.
5 V. Lacivita, N. Artrith and G. Ceder, *Chem. Mater.*, 2018, **30**, 7077–7090.
6 S. Schneider, L. G. Balzat, B. V. Lotsch and W. Schnick, *Chem.–Eur. J.*, 2023, **29**, e202202984.
7 V. Lacivita, A. S. Westover, A. Kercher, N. D. Phillip, G. Yang, G. Veith, G. Ceder and N. J. Dudney, *J. Am. Chem. Soc.*, 2018, **140**, 11029–11038.
8 H. Duan, H. Zheng, Y. Zhou, B. Xu and H. Liu, *Solid State Ionics*, 2018, **318**, 45–53.
9 N. Kamaya, K. Homma, Y. Yamakawa, M. Hirayama, R. Kanno, M. Yonemura, T. Kamiyama, Y. Kato, S. Hama, K. Kawamoto and A. Mitsui, *Nat. Mater.*, 2011, **10**, 682–686.
10 S. K. Choi, J. Han, G. J. Kim, Y. H. Kim, J. Choi and M. Yang, *Journal of Powder Materials*, 2024, **31**, 293–301.
11 A. C. Kozen, A. J. Pearse, C.-F. Lin, M. Noked and G. W. Rubloff, *Chem. Mater.*, 2015, **27**, 5324–5331.
12 A. C. Kozen, C.-F. Lin, O. Zhao, S. B. Lee, G. W. Rubloff and M. Noked, *Chem. Mater.*, 2017, **29**, 6298–6307.
13 C. S. Nimisha, K. Y. Rao, G. Venkatesh, G. M. Rao and N. Munichandraiah, *Thin Solid Films*, 2011, **519**, 3401–3406.
14 D. Cheng, T. Wynn, B. Lu, M. Marple, B. Han, R. Shimizu, B. Sreenarayanan, J. Bickel, P. Hosemann, Y. Yang, H. Nguyen, W. Li, G. Zhu, M. Zhang and Y. S. Meng, *Nat. Nanotechnol.*, 2023, **18**, 1448–1455.
15 M. Nisula, Y. Shindo, H. Koga and M. Karppinen, *Chem. Mater.*, 2015, **27**, 6987–6993.
16 A. J. Pearse, T. E. Schmitt, E. J. Fuller, F. El-Gabaly, C.-F. Lin, K. Gerasopoulos, A. C. Kozen, A. A. Talin, G. Rubloff and K. E. Gregorczyk, *Chem. Mater.*, 2017, **29**, 3740–3753.
17 C. Barbos, D. Blanc-Pelissier, A. Fave, E. Blanquet, A. Crisci, E. Fourmond, D. Albertini, A. Sabac, K. Ayadi, P. Girard and M. Lemiti, *Energy Procedia*, 2015, **77**, 558–564.
18 R. B. Nuwayhid, D. Fontecha, A. C. Kozen, A. Jarry, S. B. Lee, G. W. Rubloff and K. E. Gregorczyk, *Dalton Trans.*, 2022, **51**, 2068–2082.
19 G. Abels, I. Bardenhagen and J. Schwenzel, *Polymer*, 2020, **192**, 122300.
20 V. Klimavicius, L. Dagys, V. Klimkevičius, D. Lengvinaitė, K. Aidas, S. Balčiūnas, J. Banys, V. Chizhik and V. Balevicius, *J. Phys. Chem. B*, 2021, **125**, 12592–12602.
21 T. Polenova, R. Gupta and A. Goldbourt, *Anal. Chem.*, 2015, **87**, 5458–5469.
22 J. Schaefer and E. O. Stejskal, *J. Am. Chem. Soc.*, 1976, **98**, 1031–1032.
23 D. D. Laws, H.-M. L. Bitter and A. Jerschow, *Angew. Chem., Int. Ed.*, 2002, **41**, 3096–3129.
24 C. P. Grey and N. Dupré, *Chem. Rev.*, 2004, **104**, 4493–4512.
25 B. Reif, S. E. Ashbrook, L. Emsley and M. Hong, *Nat. Rev. Methods Primers*, 2021, **1**, 2.
26 C. Schröder, J. Ren, A. C. M. Rodrigues and H. Eckert, *J. Phys. Chem. C*, 2014, **118**, 9400–9411.
27 F. Muñoz, J. Ren, L. van Wüllen, T. Zhao, H. Kirchhain, U. Rehfuß and T. Uesbeck, *J. Phys. Chem. C*, 2021, **125**, 4077–4085.
28 B. Wang, B. C. Chakoumakos, B. C. Sales, B. S. Kwak and J. B. Bates, *J. Solid State Chem.*, 1995, **115**, 313–323.

29 Z. Wang, D. Santhanagopalan, W. Zhang, F. Wang, H. L. Xin, K. He, J. Li, N. Dudney and Y. S. Meng, *Nano Lett.*, 2016, **16**, 3760–3767.
30 C. S. Nimisha, G. M. Rao, N. Munichandraiah, G. Natarajan and D. C. Cameron, *Solid State Ionics*, 2011, **185**, 47–51.
31 H.-Y. Xia, X.-X. Wang, G.-X. Ren, W.-W. Wang, Y.-N. Zhou, Z. Shadike, E. Hu, X.-Q. Yang, J.-Y. Zheng, X.-S. Liu and Z.-W. Fu, *J. Power Sources*, 2021, **514**, 230603.
32 J. J. Kim, H. K. Kim, J. Gim, S.-B. Son and J. Song, in *Batteries*, IOP Publishing, 2021, pp. 2–1.